Euro. Jnl of Applied Mathematics (1998), *vol.* 9, *pp.* 463–483. Printed in the United Kingdom

Ploughing flows

E. O. TUCK [1] and J.-M. VANDEN-BROECK [2]

[1] *The University of Adelaide, Australia*
[2] *Department of Mathematics and Center for the Mathematical Sciences, University of Wisconsin-Madison, Wisconsin, USA*

(*Received 6 February 1996; revised 20 March 1998*)

A semi-infinite body, modelling the leading edge of a cutting tool or submerged hydrofoil, lies beneath a free surface in a uniform stream of infinitely-deep inviscid incompressible fluid flowing steadily under gravity. The body has horizontal upper and lower surfaces. The oncoming flow is partly diverted over, and partly under the body. The flow in that portion that travels over the body can be supercritical or subcritical. When it is supercritical it approaches a stream of some (to be determined) speed in a channel of some (to be determined) depth. When it is subcritical, there is also a train of waves on that stream, whose amplitude is also to be determined. Semi-analytic high-speed and low-speed solutions are obtained, and a numerical solution for finite speeds. There is a 'forbidden' intermediate speed range, within which steady flow may not be possible.

1 Introduction

The main motivation for the present study is to try to understand near-bow flows for ships or other bodies moving near a free surface. The actual ship-bow problem in general involves a splash that is thrown upward and backward (Dias & Vanden-Broeck 1993), and the task of computing this splash is quite formidable, especially if we must take into account the subsequent impact of the splash on the water ahead of the bow (c.f. Ting & Keller 1974). Fully-submerged bodies such as submarines or hydrofoils are less subject to these difficulties, but similar problems occur as their submergence is reduced toward the point where some part of the body breaks through the surface (Parkin *et al*., 1956).

When a submerged body is very close to the surface, only a thin layer of fluid passes over its top surface, and this thin layer may in fact be considered as the submerged-body equivalent of the bow splash. Although its ultimate fate is quite different, and there is no question of impact on the water ahead, the generation mechanism for the splash created by a surface-piercing bow is similar to that for the upper layer passing over a shallowly-submerged body (c.f. Tuck, 1991).

In particular, in both cases, there is a submerged stagnation point on the front face of the body, to which is attached a bifurcating streamline originating far upstream, such that all of the fluid lying above that streamline is drawn into the splash (or upper fluid layer), whereas all of the fluid lying below it passes beneath the body. An important objective of this study is determination of the depth of that bifurcating streamline, and hence the size of the splash (or upper fluid layer).

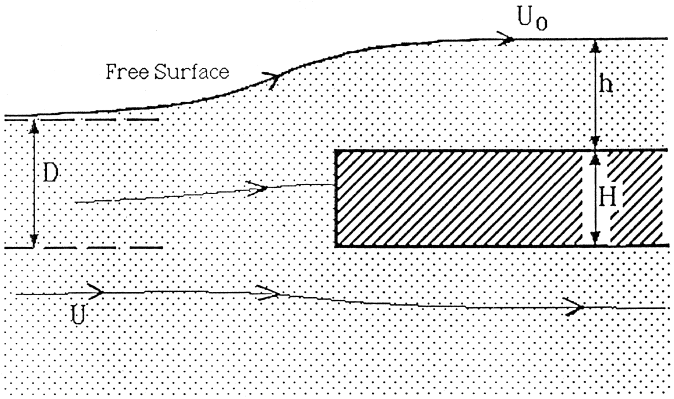

FIGURE 1. Sketch of ploughing flow, showing nomenclature.

It is also interesting to think of this class of shallowly-submerged bodies as a model of an agricultural plough, or of an industrial milling or chiselling process, or of a domestic cheese-cutter or knife. Although some of these non-naval applications are at first sight somewhat more of a solid rather than fluid nature, there is at least an analogy with the fluid case, and in some cases (e.g. in the ploughing of particulate media) a fluid model may be quite relevant. In many cases, the viscoelastic properties of the fluid can be expected to play a significant role but the present potential flow calculations provide a first step in the modelling of such applications. It is convenient to refer to this general class of flows as ploughing flows, and occasionally to the body as a plough.

If the body is being moved with constant speed U in the $-x$ direction, we view the problem in a frame of reference moving with the body, so that the body appears to be at rest with its leading edge at $x = 0$ in an otherwise uniform stream of magnitude U flowing in the $+x$ direction. Suppose that this stream has a free surface which, in the absence of the body, is the plane $y = 0$.

In the present paper, we use a simplified two-dimensional model of the geometry of the plough as sketched in Figure 1, namely an infinitely wide, semi-infinitely long, rectangular body of thickness H. Although the 90° corners of this body make it somewhat impractical, at least as a model for the naval applications, smoothing off of the corners makes little difference to the particular flow properties of interest here, and in extended work (Simakov and Tuck 1996) we have computed ploughing flows (without gravity) for a plough with an arbitrary smooth front face. Another flow option with a sharp upper corner is that the flow separates there, forming a splash jet, and this has also been investigated without gravity by Simakov and Tuck (1996). The rectangular geometry is chosen here for computational convenience, and allows certain aspects of the flow to be determined analytically by hodograph methods, c.f. Gilbarg 1960.

Suppose we submerge this rectangular body in the stream U, so that its 'draft' is D, i.e. its bottom surface is $y = -D$, and top surface is $y = -D + H$. These top and bottom surfaces are joined by a vertical front face $x = 0, -D < y < -D + H$. Usually $H < D$ so that the body is fully submerged when at rest. However, this is not a necessary requirement, and it is possible when $U > 0$ to have $H > D$, with the top surface of the

https://doi.org/10.1017/S0956792598003519 Published online by Cambridge University Press

body covered by a sheet of fluid lying wholly above the undisturbed plane $y = 0$. Such a sheet of moving fluid occurs in the flow over the top of the body for all values of the ratio H/D, and it is one of our primary tasks to compute its height h and speed U_0, neither of which is known in advance. As we shall see, there are flows for which there is a train of waves in the flow over the top of the body. In such cases we will define h and U_0 as the average depth and velocity far downstream. If $H < D$, then $h = D - H$ at rest, but the value of h may change dramatically when the body is in motion. If $H > D$, the body is surface piercing when at rest, even if submerged when in motion.

Gravity g plays an important role in this problem, and an important non-dimensional parameter is the Froude number

$$F_D = \frac{U}{\sqrt{gD}} \tag{1.1}$$

based on the body's draft, which may be considered given. The Froude number

$$F_h = \frac{U_0}{\sqrt{gh}} \tag{1.2}$$

is also of importance, but is not known in advance. The flow in the sheet of fluid passing over the top of the body is supercritical if $F_h > 1$, and subcritical if $F_h < 1$; in the latter case, it is possible for waves to appear on the free surface far downstream.

There are two extremes, where the influence of gravity relative to inertia is either dominant ($F_D \to 0$) or negligible ($F_D \to \infty$). In each of these limits, there is a simplified boundary-value problem which can be solved almost in closed form, and these limiting problems are discussed in detail below.

The problem is then solved numerically for finite F_D. Solutions are found which are supercritical, generalising the $F_D \to \infty$ limit into a range $F_D > F_2$, with the property that $F_h > 1$. There are also solutions which are subcritical, generalising the $F_D \to 0$ limit into a range $F_D < F_1$ such that $F_h < 1$. The computed range-ends F_1 and F_2 each depend only on the single ratio H/D specifying the body geometry, and in general $F_1 < F_2$ strictly. That is, there is a (generally quite wide) 'forbidden' range of speeds such that $F_1 < F_D < F_2$, within which we are unable to find solutions. Since our results have $F_h \downarrow 1$ as $F_D \downarrow F_2$, it is believed that F_2 is indeed a lower bound for existence of supercritical solutions.

For subcritical flows, there are waves on the free surface whose steepness increases as F increases. We believe that the waves break when F reaches F_1.

2 Non-dimensional formulation and conformal maps

The flow is as sketched in the complex $z = x + iy$ plane in Figure 2. Given the assumption of an inviscid incompressible fluid in steady irrotational two-dimensional motion, our task is to solve Laplace's equation for the velocity potential $\phi(x, y)$, or equivalently, to find an analytic complex potential $f(z)$. We normalise velocities so that the uniform stream is of magnitude $U = 1$, and distances so that the net volume flux in the portion of the flow going over the body is of magnitude π. Hence the flow in the complex potential $f = \phi + i\psi$ plane is as in Figure 3, with the streamline $\psi = \pi$ being the free surface, and the streamline $\psi = 0$ bifurcating from a single stagnation streamline originating upstream into two branches, on the upper and lower body surfaces. This plane is then mapped to

https://doi.org/10.1017/S0956792598003519 Published online by Cambridge University Press

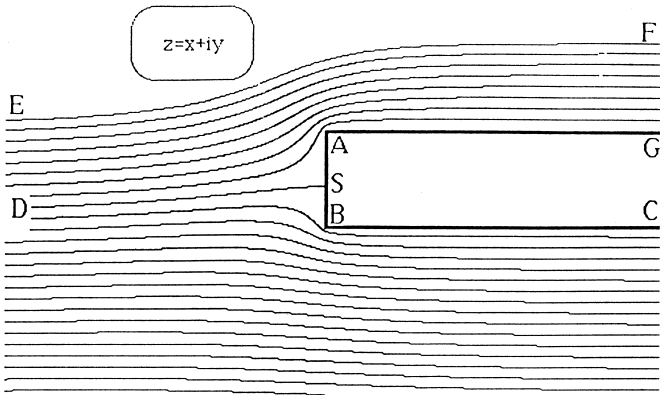

FIGURE 2. Ploughing flow in the physical $z = x + iy$ plane.

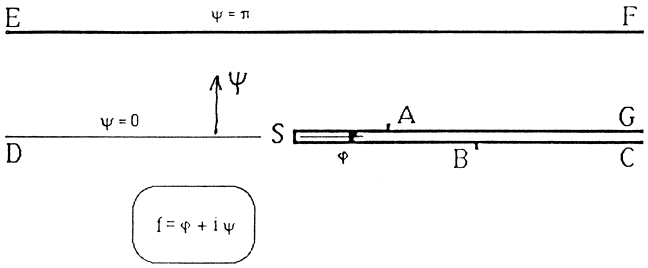

FIGURE 3. Ploughing flow in the complex potential $f = \phi + i\psi$ plane, where ϕ is the velocity potential, and ψ is the stream function.

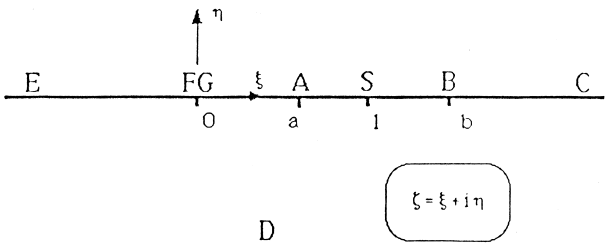

FIGURE 4. Ploughing flow in an artificial $\zeta = \xi + i\eta$ plane, such that the flow takes place in the lower half-plane $\eta < 0$.

a lower half ζ-plane by the conformal mapping

$$f = \zeta - \log \zeta \tag{2.1}$$

and the flow in the ζ-plane is as shown in Figure 4.

Prominent features of Figures 2–4 are the stagnation point S ($\zeta = 1$) and the upper and lower corners of the body, A ($\zeta = a$) and B ($\zeta = b$) respectively. These figures are sketched with the stagnation point on the forward face of the body, i.e. $a < 1 < b$, although it is also possible for the stagnation point to be located on the upper surface ($a > 1$) or lower surface ($b < 1$) of the body.

https://doi.org/10.1017/S0956792598003519 Published online by Cambridge University Press

The origin FG in the ζ-plane is actually the far downstream end of the channel flow above the body. Similarly, the region CDE at infinity in the lower half ζ-plane corresponds to the lower portion of the actual flow, with C far downstream on the lower surface of the body, D far upstream on the stagnation streamline, and E far upstream on the free surface.

The flow problem is solved in the lower-half ζ-plane, with the logarithmic hodograph

$$\Omega = \tau - i\theta = \log f'(z) = \log(u - iv) \tag{2.2}$$

as dependent variable. Note that the fluid velocity magnitude is $q = \exp(\tau)$, and θ is the angle that this velocity bears to the positive x-axis. In the numerical solution with non-zero gravity, we actually reduce the problem to an integral equation for the unknown $\theta(\xi)$ on the negative real axis $\zeta = \xi - i0, \xi < 0$, that is, on the free surface, noting that θ is wholly known on the positive real axis $\xi > 0$, i.e on the body.

The free-surface boundary condition, to be satisfied on the negative real ζ-axis, is constancy of pressure. The pressure can be related to the fluid velocity by Bernoulli's equation, and for the general case this is done later. Note that since this relationship between velocity and pressure is quadratic, the free-surface boundary condition is nonlinear, and this is the ultimate reason why gravitational free-surface problems of the present type present mathematical and computational difficulties. First we give the somewhat simpler results which apply when gravity is either negligible or dominant.

3 Analytic solution at infinite Froude number

Very large Froude number corresponds to low effective importance of gravity relative to other forces such as inertia. When gravity is absent, the free-surface boundary condition is that of unit velocity magnitude, or $\tau = 0$. Although standard hodograph tools (Gilbarg, 1960) can be used to solve the resulting boundary-value problem systematically, the simplest procedure here is to quote the solution and verify its properties. Namely, the complex velocity $\exp\Omega = u - iv$ is given by

$$u - iv = \left[\frac{\zeta^{1/2} - 1}{\zeta^{1/2} + 1}\right]\left[\frac{\zeta^{1/2} + a^{1/2}}{\zeta^{1/2} - a^{1/2}}\right]^{1/2}\left[\frac{\zeta^{1/2} + b^{1/2}}{\zeta^{1/2} - b^{1/2}}\right]^{1/2} . \tag{3.1}$$

This is an analytic function which approaches the uniform stream $u - iv = 1$ as $\zeta \to \infty$. Its properties on the real axis $\zeta = \xi - i0$ are of prime interest. It clearly has a stagnation point at $\zeta = 1$ and gives infinite velocity at $\zeta = a, b$ in such a way as to guarantee a right-angle corner at these points. For example, it is real both for $0 < \xi < a$ and $\xi > b$, so $v = 0$ on the upper and lower body surfaces, and imaginary for $a < \xi < b$, so $u = 0$ there. Finally, for $\xi < 0$, setting $\zeta^{1/2} = -i|\xi|^{1/2}$, we see that each of the three factors in (3.1) has unit magnitude, so $|u - iv| = 1$ as required.

Expression (3.1) gives velocities as a function of the artificial mapping variable ζ. To relate these to the physical plane z, we need to express z as a function of ζ, by integrating

$$\frac{dz}{d\zeta} = \frac{df}{d\zeta}\Big/\frac{df}{dz} = \frac{1 - \zeta^{-1}}{u - iv} . \tag{3.2}$$

Once this integration is done by standard numerical quadrature, we can then plot streamlines ψ =constant by finding appropriate values of ζ for each $f = \zeta - \log\zeta$. This is

https://doi.org/10.1017/S0956792598003519 Published online by Cambridge University Press

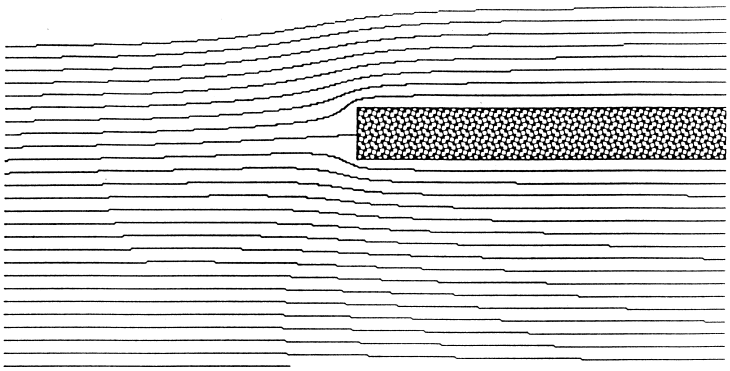

FIGURE 5. Computed streamlines with $g = 0$, at $a = 0.26644$ ($H/D = 0.5$).

actually easiest done by allowing $\beta = \arg(\zeta)$ to vary between $-\pi$ and 0, determining $|\zeta| = (\psi + \beta)/\sin\beta$ and hence ζ for each such value of β.

The above flow is characterised by just two parameters a, b. However, it is not physically acceptable for every choice of these parameters, and only one of a and b can be taken as an input, the other being determined by the relationship

$$a^{1/2} + b^{1/2} = 2. \tag{3.3}$$

The reason for this requirement can be seen by evaluating the hodograph variable θ, whose tangent v/u is the gradient of the free-surface streamline, on the negative real axis $\xi < 0$. Namely, after some manipulation of the logarithm of Eq. (3.1), we find

$$\theta = -2\arctan(-\xi)^{1/2} + \arctan\left[-\frac{\xi}{a}\right]^{1/2} + \arctan\left[-\frac{\xi}{b}\right]^{1/2}. \tag{3.4}$$

For large positive $-\xi$, i.e. far upstream, this becomes

$$\theta \to \left[2 - a^{1/2} - b^{1/2}\right](-\xi)^{-1/2} + O((-\xi)^{-3/2}). \tag{3.5}$$

But far upstream, $x \to \xi$, so (3.5) implies that the slope dy/dx of the free surface behaves like $|x|^{-1/2}$, and hence y behaves like $|x|^{1/2}$. Thus the free surface is not asymptotically plane at upstream infinity, but behaves like a parabola. That is so unless the coefficient in Eq. (3.5) vanishes, which is the relation (3.3).

This requirement is easily tested by actual computation of streamlines, including the free-surface streamline $\psi = \pi$, and indeed only when (3.3) holds are the streamlines horizontal far upstream. Figures 5 and 6 give examples of acceptable streamlines for $a = 0.26644$ and $a = 0.02013$ respectively. Some details of these streamline computations need care, e.g. it is necessary to provide an accurate starting approximation far upstream, equivalent to continuing the expansion (3.5) to at least two further terms. It is also quite a delicate computational task in the numerical integration of (3.2) to carry those streamlines which are close to the dividing streamline past the stagnation point and corners with sufficient accuracy.

An important property of the $g = 0$ solutions that satisfy Eq. (3.3) is that their non-dimensional draft is $D = \pi$. Since the stream (of unit magnitude) above the body also has height $h = \pi$, this means that the body simply displaces streamlines upward by exactly

https://doi.org/10.1017/S0956792598003519 Published online by Cambridge University Press

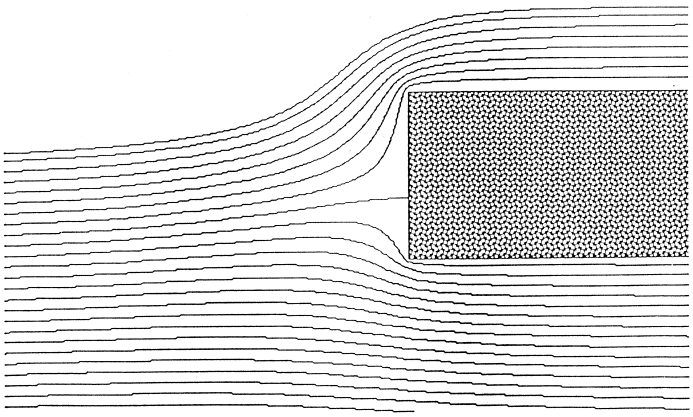

FIGURE 6. Computed streamlines with $g = 0$, at $a = 0.02013$ ($H/D = 2.0$).

its thickness H. Any fluid particle lying above the lower surface of the body when far upstream, is doomed to rise above the body.

Such is, of course, the usual expectation when chiselling or ploughing a continuous solid medium, and we now see that it also must occur in a fluid medium in the absence of significant gravitational effects. However, gravity if present does allow the possibility of some such particles falling below the body, in a liquid or particulate medium. One interpretation of our later finite-g generalisation is that it determines to what extent this phenomenon, which may be undesirable in some contexts, actually occurs.

The actual body thickness H is in the present case a function of the sole dimensionless parameter a, and is available by numerical integration of Eq. (3.2) from the bottom corner $\zeta = b$ to the top corner $\zeta = a$. For example, the case $a = 0.26644$ of Figure 5 corresponds to $H/D = 0.5$, and the case $a = 0.02013$ of Figure 6 to $H/D = 2.0$.

4 Analytic solution at zero Froude number

Very low Froude number corresponds to dominant influence of gravity relative to inertia at the free surface. The free surface is 'stiff', and cannot easily be displaced. In the limit, it becomes a plane rigid horizontal wall on which $\theta = 0$. The body lies below that plane wall, and there is a channel between it and the wall, in which there is a flow of to-be-determined velocity U_0 far downstream. The method of images indicates that this is also the flow generated by a stream U flowing toward a pair of parallel identical semi-infinite bodies.

As with the opposite extreme of the previous section, hodograph methods yield the solution readily, and indeed the present case is somewhat simpler than the previous one, such that a fully analytic solution can be written down. The complex velocity is simply

$$u - iv = (\zeta - 1)\,[(\zeta - a)(\zeta - b)]^{-1/2}\ , \tag{4.1}$$

and the resulting expression in Eq. (3.2) can be integrated explicitly to give

$$z = R - \bar{c}\log\,[R + \zeta - \bar{c}] + c^*\log\left[R + \frac{\bar{c}}{c^*}\zeta - c^*\right] - c^*\log\zeta \tag{4.2}$$

https://doi.org/10.1017/S0956792598003519 Published online by Cambridge University Press

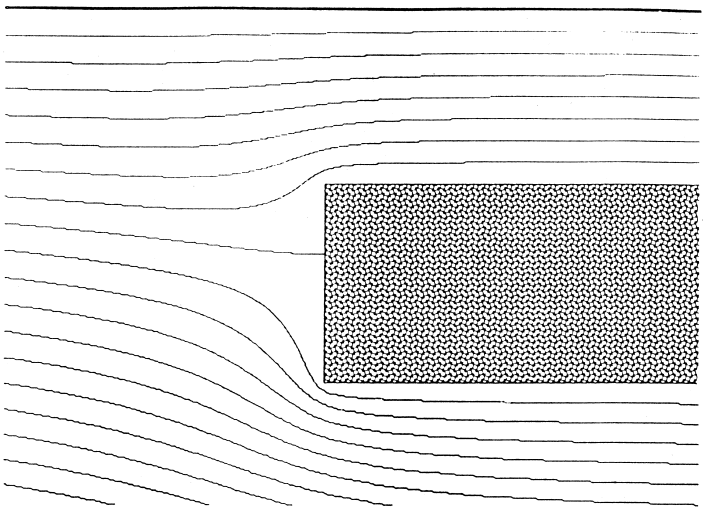

FIGURE 7. Computed streamlines with $F_D = 0$, for $(a, b) = (0.25, 4.0)$, having the same outgoing as incoming speed, $U_0 = U$.

where

$$R = [(\zeta - a)(\zeta - b)]^{1/2} \ . \tag{4.3}$$

The constants $(\bar{c}, c^*)$ in Eq. (4.2) are respectively the arithmetic and geometric means of (a, b), i.e.

$$\bar{c} = (a + b)/2, \quad c^* = \sqrt{ab}. \tag{4.4}$$

With $f = f(\zeta)$ by (2.1) and $z = z(\zeta)$ by Eq. (4.2) we have an analytic implicit solution for the required complex potential $f = f(z)$.

In particular, it is immediate that the draft of the body is $D = \pi\bar{c}$, and the height of the channel above the body is $h = \pi c^*$, so the height of the body is $H = D - h = \pi(\bar{c} - c^*)$. The velocity of the outgoing stream above the body is $U_0 = 1/c^*$. Thus, irrespective of the particular non-dimensionalisation used to derive these results, we have

$$H/D = 1 - c^*/\bar{c} \quad \text{and} \quad U_0/U = 1/c^*. \tag{4.5}$$

Streamlines can again be plotted directly, as in the previous section, but more easily since there is no numerical integration to be performed.

Given the assumption that the free surface is fully rigid, and can support any pressure, the present flow provides a fully-acceptable two-parameter family, with both a and b (or equivalently both $\bar{c}$ and c^*) as input parameters. However, there are two distinguished one-parameter sub-families, namely that with $c^* = 1$ and that with $\bar{c} = 1$. The former sub-family is of some minor interest in that $U_0 = 1$, so that the outgoing stream has the same velocity (and hence in the absence of gravity the same pressure) as the incoming stream $U = 1$. Figure 7 shows an example of such a flow, with $(a, b) = (0.25, 4)$. Note that in this and any other sub-family except that to be discussed below, the effect of the body is felt as an apparent source at infinity far beneath the body, and those streamlines going below the body are deflected downward by it.

The sub-family with $\bar{c} = 1$ is however such that there is no apparent source at infinity.

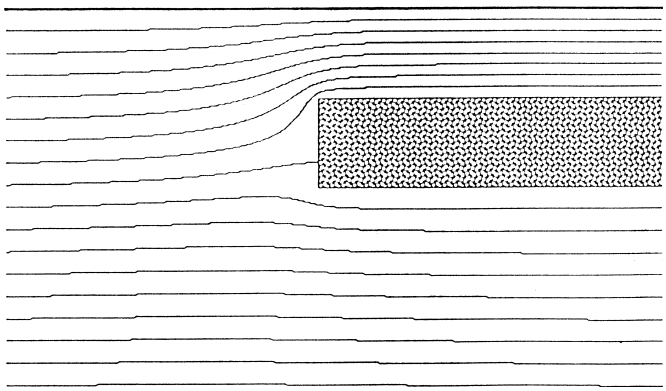

FIGURE 8. Computed streamlines with $F_D = 0$, for $(a, b) = (0.134, 1.866)$, such that $H/D = 0.5$ and $U_0/U = 2.0$

This is explicitly seen by a far-field expansion of Eq. (4.1), namely

$$u - iv = 1 + (\bar{c} - 1)\zeta^{-1} + O(\zeta^{-2}) \tag{4.6}$$

in which the term in $\zeta^{-1} \approx z^{-1}$ represents a source. If $\bar{c} = 1$, this term is absent. Physically, with $U_0 > 1$, there is just sufficient extra flux absorbed into the stream above the body to prevent downward deflection of those streamlines passing below the body. Figure 8 shows an example of such a flow, with $(a, b) = (0.134, 1.866)$ or $(\bar{c}, c^*) = (1.0, 0.5)$, i.e. thickness $H/D = 0.5$ and channel speed $U_0/U = 2.0$.

If the plane boundary were genuinely rigid, a flow in the last category could only be produced by suction in the downstream channel, since ('neglecting' gravity) an increased velocity $U_0 > 1$ demands a decreased pressure. However, gravity is dominant, not negligible in this flow, and it turns out that this sub-family is the one that is approached in the true limit as the Froude number tends to zero. In that limit, the extreme stiffness of the free surface allows it to bear the increased velocity by a small deflection.

5 The Nekrasov integral equation for non-zero gravity

The free-surface boundary condition with gravity is constancy of pressure, or from Bernoulli's equation,

$$\frac{1}{2}(u^2 + v^2) + gy = \frac{1}{2}\,. \tag{5.1}$$

In the ζ-plane, this holds for all real negative ζ, and can be differentiated with respect to ζ and manipulated to the form

$$\tau(\zeta) = \frac{1}{3}\log\left[1 - 3g\int_{-\infty}^{\zeta}\left(1 - \frac{1}{\xi}\right)\sin\theta(\xi)d\xi\right]\,. \tag{5.2}$$

A second relationship between the harmonic conjugates τ and θ follows from Cauchy's theorem, which for real ζ states

$$\tau(\zeta) = \frac{1}{\pi}\int_{-\infty}^{\infty}\frac{\theta(\xi)}{\xi - \zeta}d\xi \tag{5.3}$$

https://doi.org/10.1017/S0956792598003519 Published online by Cambridge University Press

where the integral is a Cauchy principal value. In Eq. (5.3), θ is known for $\xi > 0$, but is to be determined for $\xi < 0$. In particular, for the rectangular box geometry, $\theta = 0, \pi/2, -\pi/2$ and 0, for $0 < \xi < a$, $a < \xi < 1$, $1 < \xi < b$ and $\xi > b$ respectively. Thus Eq. (5.3) becomes

$$\tau(\zeta) = \frac{1}{\pi}\int_{-\infty}^{0} \frac{\theta(\xi)}{\xi - \zeta} d\xi + \frac{1}{2}\log\left|\frac{(1-\zeta)^2}{(a-\zeta)(b-\zeta)}\right| . \tag{5.4}$$

Equating Eqs. (5.2) and (5.4) yields a nonlinear singular integral equation for $\theta(\xi)$ on $\xi < 0$, sometimes called a Nekrasov equation (Wehausen and Laitone 1960, p.750). Explicitly, this equation is

$$\frac{1}{3}\log\left[1 - 3g\int_{-\infty}^{\zeta}\left(1 - \frac{1}{\xi}\right)\sin\theta(\xi)d\xi\right] = \frac{1}{\pi}\int_{-\infty}^{0}\frac{\theta(\xi)}{\xi-\zeta}d\xi + \frac{1}{2}\log\left|\frac{(1-\zeta)^2}{(a-\zeta)(b-\zeta)}\right| \tag{5.5}$$

or on exponentiation,

$$1 - 3g\int_{-\infty}^{\zeta}\left(1 - \frac{1}{\xi}\right)\sin\theta(\xi)d\xi = \left|\frac{(1-\zeta)^2}{(a-\zeta)(b-\zeta)}\right|^{3/2}\exp\left[\frac{3}{\pi}\int_{-\infty}^{0}\frac{\theta(\xi)}{\xi-\zeta}d\xi\right] . \tag{5.6}$$

It is only necessary to provide appropriate numerical quadratures for the integrals, and to collocate on a suitable grid of values of ζ, to reduce the Nekrasov equation to a solvable set of nonlinear algebraic equations. Such a procedure is described in the following section.

It is interesting to observe small-g and large-g limits of Eq. (5.5). Note that since we have non-dimensionalised velocities and lengths by setting the incident stream $U = 1$, and the flux in the outgoing channel flow equal to π, the parameter g in Eq. (5.5) is actually a non-dimensional measure of gravity, equivalent to an inverse square Froude number.

The high Froude number limit is thus $g = 0$, in which case the left-hand side of Eq. (5.5) vanishes, i.e. $\tau = 0$ as required. But then θ is determined simply by finding the inverse Hilbert transform of the logarithmic expression on the right of Eq. (5.5), and it is not hard to verify that this is given by Eq. (3.4).

On the other hand, the low Froude number limit corresponds to letting $g \to \infty$ in Eq. (5.5). This immediately demands from the left-hand side that $\theta \to 0$, whereupon τ is given by the logarithmic expression on the right. Analytically continuing this expression gives the complex velocity as in Eq. (4.1).

6 Numerical procedure for solution of the Nekrasov equation

In principle, any grid on $-\infty < \xi < 0$ can be used. This consists of a set of nodes $\xi = \xi_j$ and collocation points ζ_j, with $j = 0, 1, \ldots, N$ and $\xi_{j-1} < \zeta_j < \xi_j$. There is a need for a concentration of nodes near $\xi = 0$. For this purpose, we have used both a power law grid, with $\xi_j \propto (N - j)^\alpha$ for some $\alpha > 1$, and a grid which is constructed to be of equal spacing in ϕ, i.e. where $\xi = \xi_j$ is obtained by numerical solution of the transcendental equation

$$\xi - \log|\xi| = \phi = X_- + (j/N)(X_+ - X_-) \tag{6.1}$$

for some range (X_-, X_+) of ϕ approximating $(-\infty, \infty)$. The collocation points are then mid-points with respect to ϕ, i.e. $\xi = \zeta_i$ satisfy grid (6.1) with j replaced by $(i - 1/2)$.

The power law grid is in principle good for supercritical cases, if α is carefully chosen,

https://doi.org/10.1017/S0956792598003519 Published online by Cambridge University Press

because then the approach of θ to zero far downstream is via such a power of ξ, as $\xi \to 0$. However, the uniform-ϕ grid (6.1) proved to be just as good in the supercritical case, and better for the subcritical case, so was preferred. Note that as $\xi \to 0$, or j becomes large, the grid spacing in ξ prescribed by grid (6.1) tends to zero exponentially rapidly. In practice, $(X_-, X_+) = (-30, 15)$ and $N = 80$ was adequate for three-figure accuracy in most cases.

The N unknowns are $\theta_j = \theta(\xi_j), j = 1, 2, \ldots, N-1$, and b. These N unknowns are determined using the NAG routine C05NBF to solve the N nonlinear algebraic equations obtained by forcing the Nekrasov equation (5.5) to hold at the N collocation points $\zeta = \zeta_i, i = 1, 2, \ldots, N$. As at $g = 0$, we assume that only one of the two parameters, here a, can be fixed in advance, and allow the other parameter b to be determined by the program.

The end values of θ are determined separately; in particular, $\theta_0 = \theta(\xi_0)$ is assumed inverse-square extrapolable from θ_1, as discussed further below. The value of $\theta_N = \theta(0)$ is not actually needed for the integral on the left of Eq. (5.5), and plays only a relatively minor role in the integral on the right of Eq. (5.5), so long as the grid spacing approaches zero as $\xi \to 0$. In the supercritical case, we can be sure that $\theta(0) = 0$, and this is assumed. This assumption is also accurate in the subcritical case so long as there are no waves, but when waves are present in the channel flow far downstream, $\theta(0)$ is undefined.

Choices for the upstream grid commencement point $\xi_0 \approx X_-$ and corrections for behaviour of the flow beyond that distance upstream turn out to be of some importance. It is not hard to see that for all non-zero g (in contrast to the case $g = 0$ where Eq. (3.5) indicates inverse 3/2 power decay), the angle θ decays like the inverse square of distance upstream, and hence like ξ^{-2}. We write for large $|\xi|$ therefore

$$\theta \approx \frac{B}{g}\xi^{-2} + O(\xi^{-3}\log|\xi|) \tag{6.2}$$

for some constant B to be determined. Now if B is known, in both integrals (5.2) and (5.4) we can replace $-\infty$ by ξ_0, correcting explicitly for this approximation by estimating the contributions to these integrals from the range $(-\infty, \xi_0)$ by use of Eq. (6.2).

The corresponding far-upstream asymptote for the harmonic conjugate to θ is

$$\tau \approx B\zeta^{-1} + O(\zeta^{-2}\log|\zeta|) \tag{6.3}$$

and (after some numerical experimentation) it was found that the best way to carry out the truncation correction during the computation was to fit Eq. (6.3) to the furthest upstream collocation value of τ, i.e. to determine a provisional value of B by setting $\tau(\zeta_1) = B/\zeta_1$, and then to use that value of B in Eq. (6.2) as described above. This procedure has the effect of providing a very smooth upstream termination to the computational domain, so avoiding any tendency to generate spurious upstream waves at that point. However, once final converged solutions for $\theta(\xi)$ are achieved, a more accurate final estimate for B itself is obtainable by letting $\zeta \to -\infty$ in Eq. (5.4), i.e.

$$B = -\frac{1}{\pi}\int_{-\infty}^{0} \theta(\xi)d\xi - 1 + \frac{1}{2}(a+b). \tag{6.4}$$

The actual numerical quadratures used are as follows. For the 'running' integral in Eq. (5.2), we first fit a quadratic function of ξ to the full integrand at each set of three

https://doi.org/10.1017/S0956792598003519 Published online by Cambridge University Press

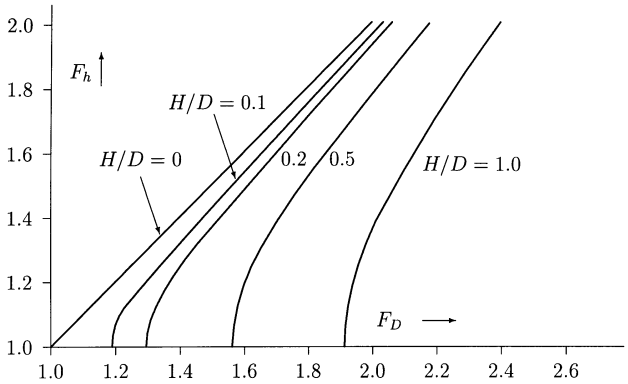

FIGURE 9. Outgoing supercritical Froude number $F_h = U_0/\sqrt{gh}$ based on channel depth, as a function of (high) input Froude number $F_D = U/\sqrt{gD}$ based on body draft, for various values of body dimensions H/D.

nodes $(\xi_{i-1}, \xi_i, \xi_{i+1})$. Then we integrate that quadratic over a collocation region (ζ_{i-1}, ζ_i) which is entirely interior to the above nodal set, enabling us to advance the integration very accurately from $\zeta = \zeta_{i-1}$ to $\zeta = \zeta_i$. On the other hand, for the full-range integration of Eq. (5.4) (and (6.4)), we simply assume that $\theta(\xi)$ is stepwise linear on each interval (ξ_{j-1}, ξ_j).

Once the N unknowns (θ_j, b) are determined, all required physical-plane parameters are available by simple post-processing operations. In particular, it follows from the far-field asymptote (6.3) that the body's draft is given by $D = \pi(1 + B)$, where B is determined from Eq. (6.4). The body's height H is obtained by numerical integration of Eq. (3.2) from $\zeta = b$ to $\zeta = a$. In practice, it proved convenient to build in a fixed (input) value of the ratio H/D, simply by adding an extra unknown (a) to the list of unknowns handled by C05NBF, and an extra equation H/D =given.

For each given body, this leaves the (non-dimensional) gravitational constant g as the only input parameter, and results were obtained by varying g within suitable ranges. Generally, smaller (order 0.1) input g yielded supercritical outputs, and larger (order 10) g subcritical outputs, which we now describe.

7 Super-critical results

The program was mainly designed for small-g use, and generally behaved very well in that range. The only potential problem occurs with the upstream truncation correction, and, as described earlier, a tendency to generate spurious upstream waves was alleviated by careful provisional estimation of the coefficient B in the truncation correction. Any residual difficulties are solved simply by using a bigger and bigger value of $|X_-|$, but $X_- = -30$ was adequate.

The results for the free-surface shape are in close agreement with the $g = 0$ results of § 3 when $g \approx 0.001$ or less. As we increase g beyond that range, we compute each time the Froude numbers F_D and F_h, and Figure 9 shows a graph of F_h versus F_D, for various bodies specified by their H/D values. The $g = 0$ limit would correspond to $F_h \to \infty$ as

https://doi.org/10.1017/S0956792598003519 Published online by Cambridge University Press

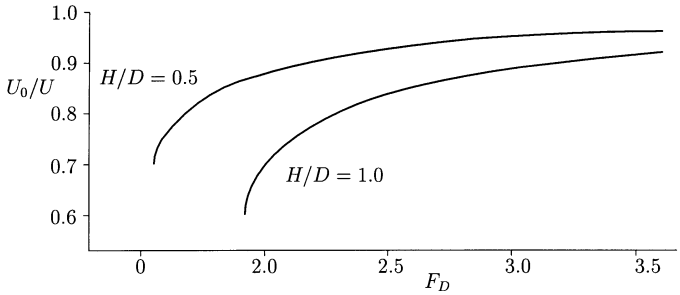

FIGURE 10. Plot of the lowest possible Froude number based on draft $F_D = F_2$ at which supercritical solutions can occur, as a function of body dimensions H/D.

$F_D \to \infty$ on that graph. In that limit, irrespective of the value of H/D, we have seen that $U_0 = U$ and $h = D$, so that all curves in Figure 9 approach the 45° line $F_h = F_D$. It is also true that the smaller is H/D, the closer is the curve to this line for all F_D, since as $H/D \to 0$, the plough becomes slender and ultimately approaches an infinitely thin knife which does not disturb the stream, and again $U_0 = U$ and $h = D$. This zero-disturbance limit of a horizontal semi-infinite submerged flat plate differs from a similar geometry examined by Vanden-Broeck and Dias (1991) where there was a non-trivial flow in that limit induced by pressure differences (the configuration considered by Vanden-Broeck and Dias (1991) differs from ours because it is in finite depth and the flow is supercritical upstream).

For finite $F_D > 1$ and non-zero H/D, we find $F_h < F_D$, and for each H/D, supercritical flows are obtained only when $F_D > F_2$ for some $F_2 > 1$. That is, F_h approaches the critical value $F_h = 1$ as F_D approaches from above a limiting value $F_D = F_2$ which depends only on the ratio H/D. Figure 10 shows F_2 as a function of H/D. Equivalently, there is a critical value $g = g_2$ of the input gravitational parameter such that $F_h \to 1$ as $g \to g_2$ from below. The program is unable to generate solutions when the input g lies in a range of values just above g_2, or equivalently for $F_h < F_2$. Since the graph in Figure 9 of F_h versus F_D becomes vertical as F_D approaches F_2, it seems very likely that there are no solutions at all in a range of F_D just below F_2.

In view of this locally-vertical character to the graphs in Figure 9, it is also possible (c.f. Vanden-Broeck, 1987; Dias & Vanden-Broeck, 1989; Asavanant & Vanden-Broeck, 1994) that these curves actually turn back into a parameter region with $F_h < 1$ and $F_D > F_2$. If this were to happen, it would indicate a lack of uniqueness, with both supercritical and subcritical solutions in existence at the same given value of the input parameter $F_D > F_2 > 1$. However, no subcritical solutions with $F_D > 1$ have been found in the present study.

In any case, Figure 10 gives for each body, the lowest draft-based Froude number F_2 at which a smooth steady supercritical ploughing flow can take place. In practice, presumably some kind of hydraulic jump or unsteady flow will occur as the critical speed F_2 is approached from above.

Various other output quantities of interest are also available. For example, Figure 11 gives, for various H/D, the variation with Froude number F_D of the outgoing speed U_0 relative to the incoming speed U. For H/D values of the order of 1, there is a significant

https://doi.org/10.1017/S0956792598003519 Published online by Cambridge University Press

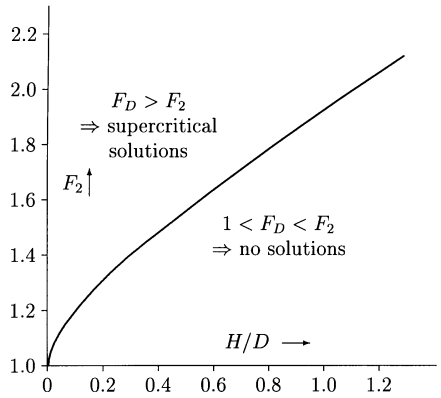

FIGURE 11. Outgoing channel-flow velocity as a function of Froude number based on draft.

drop in U_0 as F_D decreases, noting that $U_0 \to U$ as $F_D \to \infty$. For example, at $H/D = 1.0$, the outgoing speed drops to about 60% of the incoming speed as $F_D \to F_2$, with most of this drop occurring quite close to F_2. Meanwhile, however, the actual height h of the outgoing stream changes only a relatively small amount from the value $h = D$ which it must take in the large-F_D limit. In fact, as F_D decreases, at first h decreases below H, by an amount of less than 10%, before increasing again until it finally exceeds H by about 10% close to the limiting Froude number F_2. Clearly the main cause for the drop in the outgoing Froude number F_h is stream speed reduction, not stream height increase. Indeed, the whole free-surface shape is never more than about 10% different from the $g = 0$ case discussed in § 3.

We conclude this section by mentioning that analytical informations on the forces acting on the submerged object can obtained by using the principle conservation of momentum and Bernoulli equation. The details are presented in the Appendix.

8 Sub-critical results

The numerical scheme of § 6 was primarily designed for supercritical flows. It also gives also good results for subcritical flows at low Froude numbers, but becomes sensitive as soon as waves appear on the downstream free surface. An alternative version of the numerical scheme was then derived which enabled us to compute accurate solutions with waves. We shall refer to this new version as scheme B. When there are no waves, the results predicted by scheme B are in good agreement with those given by the scheme of § 6.

To derive scheme B, we first rewrite Eq. (5.1) as

$$\frac{1}{2}e^{2\tau} + g\int_{-\infty}^{\phi} e^{-\tau(\phi_o)} \sin\theta(\phi_o) d\phi_o = \frac{1}{2}. \tag{8.1}$$

We define the mean depth h and the mean velocity U_0 in the downstream flow by

$$\frac{1}{2}\frac{\pi^2}{h^2} + g(h - D + H) - \frac{1}{2} = 0. \tag{8.2}$$

If the flow approaches a uniform stream in the far field, then h is the actual depth and

https://doi.org/10.1017/S0956792598003519 Published online by Cambridge University Press

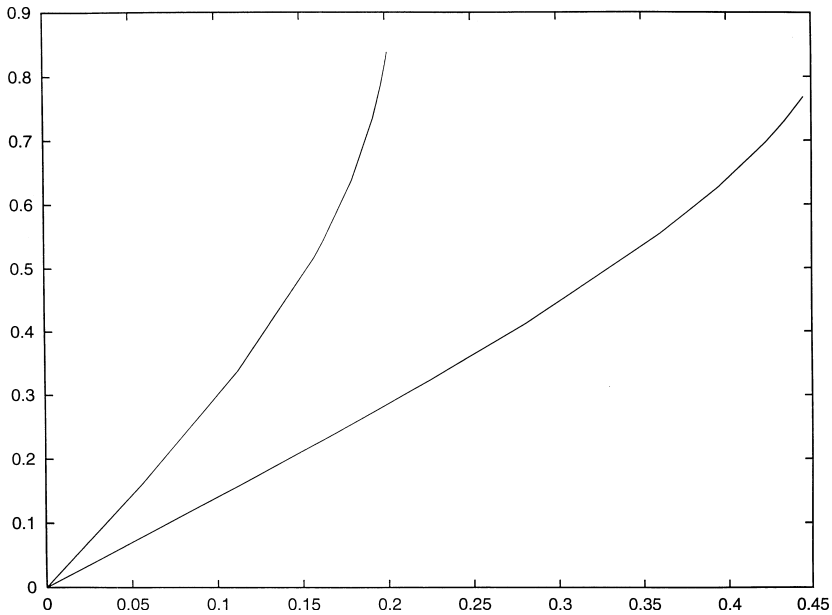

FIGURE 12. Values of F_h versus F_D for $H/D = 0.5$ (top curve) and $H/D = 0.2$ (bottom curve).

U_0 the actual velocity of that stream. This can easily be shown as follows. Let us denote by d, the uniform depth in the far field. Since the dimensionless flux in the sheet of fluid on top of the object is π, the velocity in the far field is then π/d. Substituting this value of the velocity in Eq. (5.1), we find that the difference of ordinates between the levels of the free surface far downstream and far upstream is

$$\frac{1}{2g}\left[1-\left(\frac{\pi}{d}\right)^2\right]$$

Equating this value to $d + H - D$ yields Eq. (8.2) with $d = h$, and

$$U_0 = \frac{\pi}{h}. \tag{8.3}$$

Therefore we can interpret h in Eq. (8.2) as the undisturbed depth far downstream.

Equations (5.4) and (8.1) define a nonlinear integral equation for the unknown function θ on the free surface. The main difference in the approach of scheme B is that we do not combine Eq. (5.4) and Eq. (8.1) into a Nekrasov equation as we did in § 5. The rest of the numerical procedure is similar to that of § 6.

We used the numerical scheme B to compute solutions for various values of g and H/D. We present results for $H/D = 0.2$ and $H/D = 0.5$. Most of the calculations were done with $N = 540$.

In Figure 12, we show values of F_h versus F_D for $H/D = 0.2$ and $H/D = 0.5$. Typical free surface profiles are shown in Figures 13–18. Our results show that there is a train of waves on the downstream free surface. For F small, the waves are of very small amplitude and the free surfaces are essentially flat (see Figure 13 for an example). Such solution can also be computed by the scheme of § 6. In Figure 14, the waves are close to linear sine

https://doi.org/10.1017/S0956792598003519 Published online by Cambridge University Press

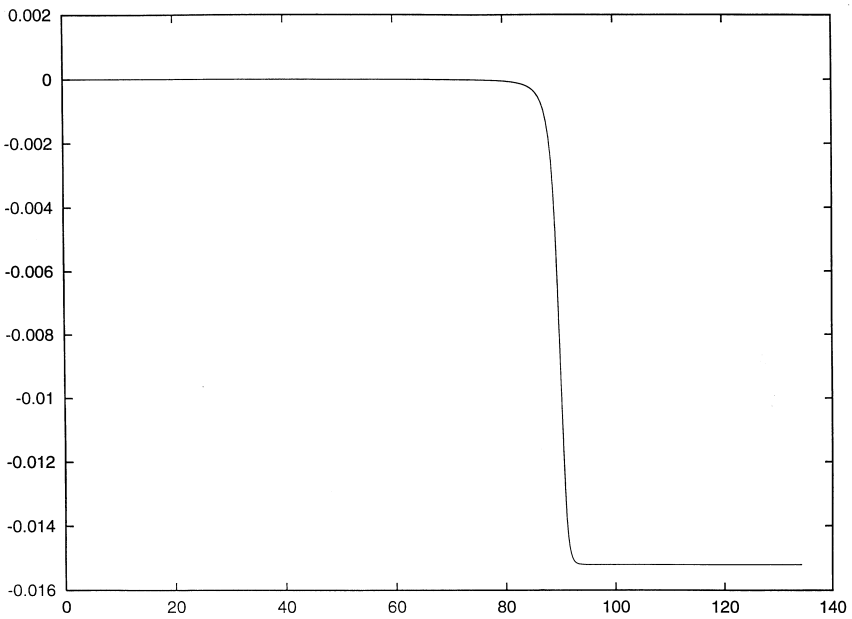

FIGURE 13. Computed free surface profile for $H/D = 0.5$. The values of the Froude numbers are $F_h = 0.16$ and $F_D = 0.056$.

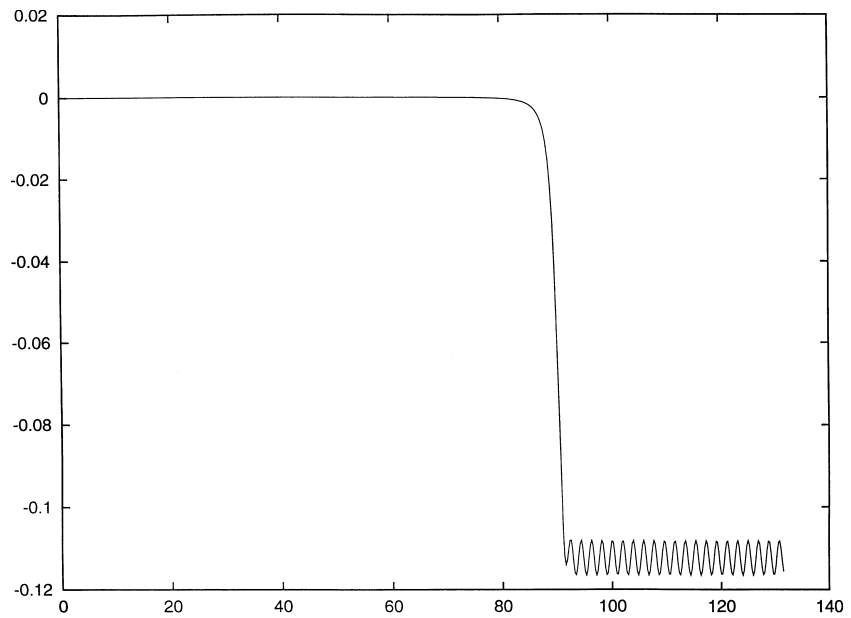

FIGURE 14. Computed free surface profile for $H/D = 0.5$. The values of the Froude numbers are $F_h = 0.44$ and $F_D = 0.14$.

https://doi.org/10.1017/S0956792598003519 Published online by Cambridge University Press

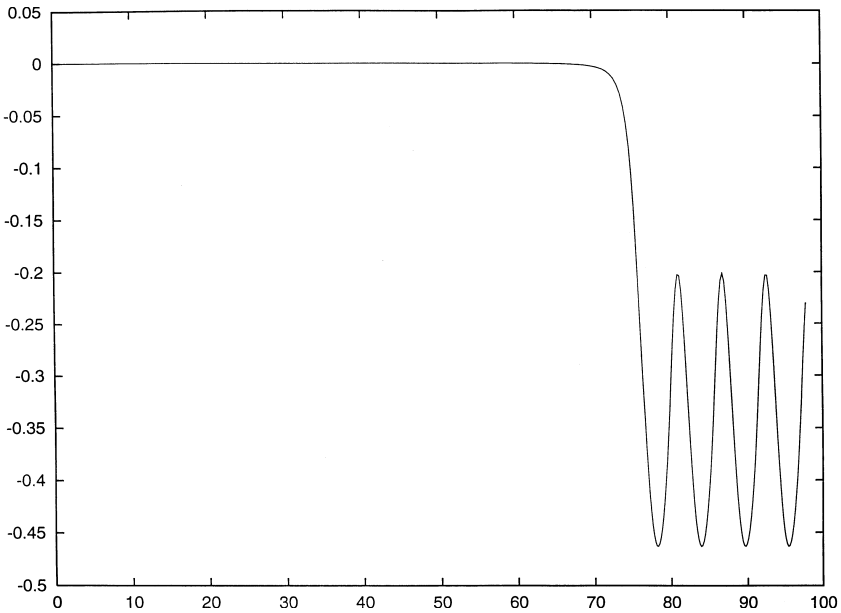

FIGURE 15. Computed free surface profile for $H/D = 0.5$. The values of the Froude numbers are $F_h = 0.79$ and $F_D = 0.198$.

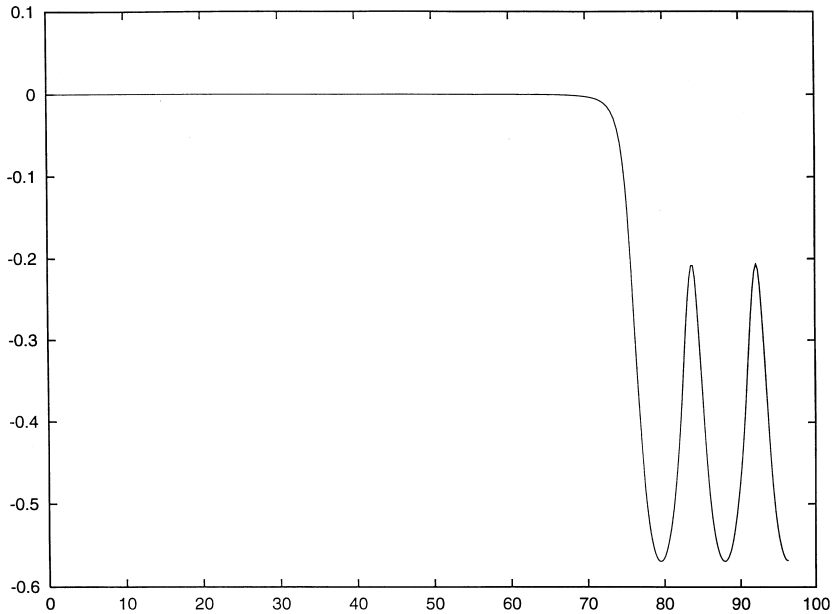

FIGURE 16. Computed free surface profile for $H/D = 0.5$. The values of the Froude numbers are $F_h = 0.83$ and $F_D = 0.201$.

https://doi.org/10.1017/S0956792598003519 Published online by Cambridge University Press

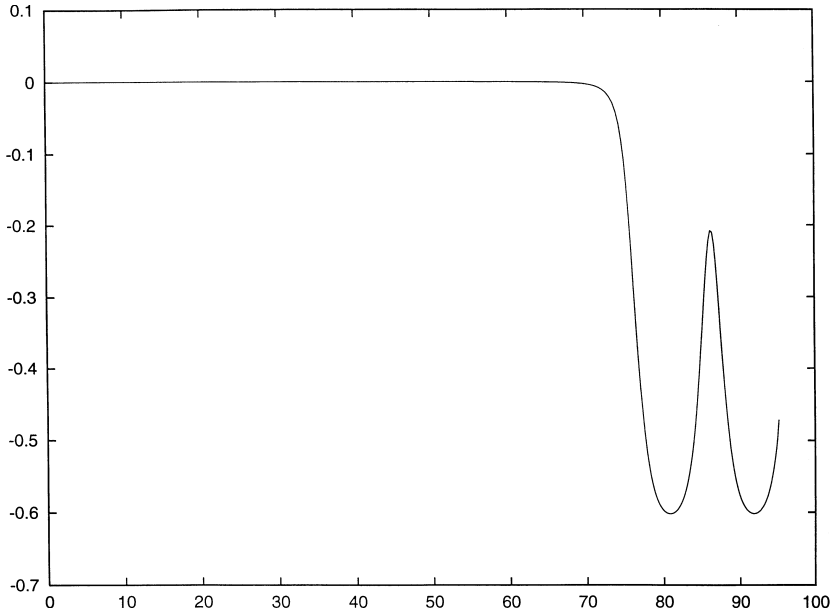

FIGURE 17. Computed free surface profile for $H/D = 0.5$. The values of the Froude numbers are $F_h = 0.84$ and $F_D = 0.201$.

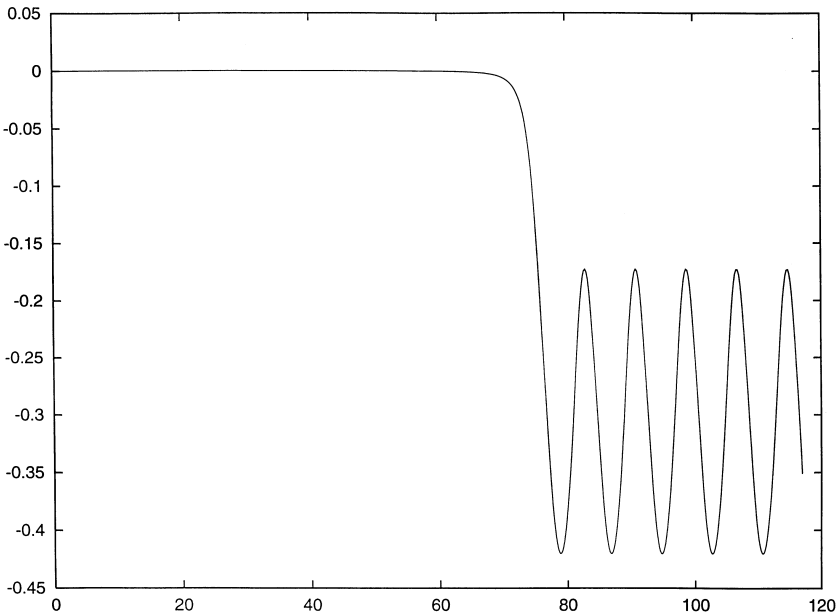

FIGURE 18. Computed free surface profile for $H/D = 0.2$. The values of the Froude numbers are $F_h = 0.73$ and $F_D = 0.43$.

https://doi.org/10.1017/S0956792598003519 Published online by Cambridge University Press

waves. However in Figures 16 and 17 the waves are clearly nonlinear with broad troughs and sharp crests.

As F_h increases, the wavelength of the waves increases and more and more mesh points are needed for the computations. We stopped the calculations around $F_h = 0.8$.

The numerical results of Figures 12–18, show that the waves steepened as F_D increases. This suggests that there is an upper bound F_1 at which the waves break and that the subcritical solutions are confined to $F_D < F_1$.

9 Conclusion

We have presented here semi-analytic solutions at zero and infinite Froude number, and numerical solutions via integral equations at finite Froude number. These results are for an idealised sharp-cornered body. For general smoother bodies, other numerical techniques, e.g. desingularised boundary integral equations, as in Scullen & Tuck (1995), may be preferable, and are under investigation.

However, the general conclusion of this paper is unlikely to be affected by such improvements. Namely, there are both high and low Froude number solutions. The former involve smooth and wave-less supercritical flows above the body, and exist only above a certain well-defined speed. The latter exist only below a certain speed, and involve a subcritical stream above the body, on which waves occur.

A somewhat similar conclusion about existence of both supercritical and subcritical solutions was obtained by King & Bloor (1987) in a study of flow over a step. That flow is analogous to the upper portion of the flow in the present geometry, namely that lying above the location of the stagnation streamline. However, for a step geometry in water that is of finite depth both upstream and downstream as studied by King & Bloor (1987) there is no doubt about when to expect supercritical and when to expect subcritical flow over the step; subcritical upstream yields subcritical downstream, and supercritical upstream yields supercritical downstream. In the present case, the depth upstream is infinite, and the Froude number F_D based on body draft has no particular indicative significance. Nevertheless, we have found supercritical solutions only for relatively high F_D, and subcritical solutions only for relatively low F_D.

Appendix A

In this appendix, we present an analytical formula for the forces acting on the submerged object. The analysis assumes that there are no waves on the free surface. Therefore the results apply directly only to the supercritical flows of § 7.

The principle of conservation of momentum in dimensional variables implies that

$$\int \left[\mathbf{V}(\mathbf{V}.\mathbf{n}) + gy\mathbf{n} + \frac{p}{\rho}\mathbf{n} \right] ds = 0 \tag{A 1}$$

Here $\mathbf{V}$ is the vector velocity, p the pressure and ρ the density. The integral is along a closed contour inside the fluid, $\mathbf{n}$ is the outward unit normal and s is the arclength. We choose the contour to consist of the free surface S_f, a vertical line S_l at $x = -\infty$, a horizontal line S_h at $y = -\infty$, a vertical line S_r^1 at $x = \infty$ from the top of the body to the

https://doi.org/10.1017/S0956792598003519 Published online by Cambridge University Press

free surface, a vertical line S_r^2 at $x = \infty$ from the bottom of the body to $y = -\infty$ and the surface S_b of the body. Furthermore, Bernoulli's equation in dimensional variables gives the additional relation

$$\frac{1}{2}(u^2 + v^2) + gy + \frac{p}{\rho} = \frac{U^2}{2} \tag{A 2}$$

Taking the component of (A.1) along the x-axis we have

$$\int \left[V_x(\mathbf{V}.\mathbf{n}) + gyn_x + \frac{p}{\rho} n_x \right] ds = 0 \tag{A 3}$$

Here V_x and n_x are, respectively, the components of $\mathbf{V}$ and $\mathbf{n}$ in the x-direction. It is convenient to replace S_h by a horizontal line at $y = -L - D$ where L is very large and D is defined in Figure 1.

Along S_l, $u = U$, $v = 0$, $n_x = -1$ and equation (A.2), gives $p/\rho + gy = 0$. Therefore the contribution to Eq. (A.3) from S_l is

$$-U^2(D + L) \tag{A 4}$$

Similarly, the contributions to (A.3) from S_r^1 and S_r^2 are

$$\left(\frac{U^2}{2} + \frac{U_0^2}{2} \right) h + U^2 L \tag{A 5}$$

Along S_f, $p = 0$, $\mathbf{V}.\mathbf{n} = 0$ and $n_x ds = -dy$. Using these results we find that the contribution to Eq. (A.3) from S_f is

$$-\frac{g}{2}(h + H - D)^2 \tag{A 6}$$

Along S_h and along the top and bottom parts of the body $\mathbf{V}.\mathbf{n} = 0$ and $n_x = 0$. Therefore these surfaces do not contribute to (A.3). Finally, the contribution to Eq. (A.3) from the front part of the object is

$$-U^2 D C_D - \frac{g}{2}(D - H)^2 + \frac{g}{2} D^2 \tag{A 7}$$

Here

$$C_D = \frac{1}{U^2 D} \int \frac{p}{\rho} dy \tag{A 8}$$

is the drag. The integral in Eq. (A.8) is on the the front part of the object. Combining the contributions (A.4)–(A.7) we obtain

$$C_D = \frac{1}{2F_D^2} \left[-1 - 2\left(\frac{H}{D}\right)^2 - \alpha^2 + 4\frac{H}{D} - 2\alpha\frac{H}{D} + 2\alpha - 2F_D^2 + \alpha F_D^2 + F_h^2 \alpha^2 \right] \tag{A 9}$$

Here $\alpha = h/D$. This quantity can be evaluated by using Eq. (A.2) on the free surface at $x = \pm\infty$. This gives

$$\alpha = \frac{F_D^2 + 2 - 2\frac{H}{D}}{F_h^2 + 2} \tag{A 10}$$

Formulae (A.9) and (A.10) define the drag analytically as a function of F_D, F_h and H/D. Numerical values can be obtained from the data of Figure 9. In the particular case $g \to 0$, (A.9) gives $C_D = -1 + \alpha$. On the other hand the results of § 3 show that $\alpha = 1$ when $g = 0$. Therefore $C_D = 0$ when $g = 0$.

https://doi.org/10.1017/S0956792598003519 Published online by Cambridge University Press

The transverse force on the body is in general unbounded unless the difference of pressure Δp across the object at $x = \infty$ is zero. From Bernoulli's equation (A.2), we obtain

$$\Delta p = \frac{U^2 - U_0^2}{2}\rho - \rho g H \tag{A 11}$$

Using (1.1), (1.2) and (A.11) we find that $\Delta p = 0$ when

$$2\frac{H}{D} = F_D^2 - F_h^2\alpha \tag{A 12}$$

where α is given by (A.10). Substituting Eq. (A.10) into Eq. (A.12) gives a necessary relation between F_D, F_h and H/D for the transverse force on the object to be finite. It can be shown that this relation is not satisfied in general for the numerical data of Figure 9. This does not invalidate our calculations since in the applications mentioned in the introduction the flow of Figure 1 is viewed as a local solution near the leading edge of a long object of finite length. For such a finite object, the condition $\Delta p = 0$ does not apply and the transverse force can be expected to be finite, although it cannot be calculated from the local solution presented here.

References

[1] Asavanant, F. & Vanden-Broeck, J.-M. (1994) Free–surface flows past a surface-piercing object of finite length. *J. Fluid Mech.* **273**, 109–124.

[2] Dias, F. & Vanden-Broeck, J.-M. (1993) Nonlinear bow flows with spray. *J. Fluid Mech.* **255**, 91–102.

[3] Gilbarg, D. (1960) Jets and cavities. In: S. Flugge (ed)., *Handbuch der Physik* **9**, 311–445. Springer-Verlag.

[4] King, A. C. & Bloor, M. I. G. (1987) Free–surface flow over a step. *J. Fluid Mech.* **182**, 193–208.

[5] Parkin, B. R., Perry, B. & Wu, T. Y.-T. (1974) Pressure distribution on a hydrofoil running near the water surface. *J. Appl. Phys.* **27**, 232–240.

[6] Scullen, D. & Tuck, E. O. (1995) Nonlinear free–surface flow computations for submerged cylinders. *J. Ship Res.* **39**, 185–193.

[7] Simakov, S. & Tuck, E. O. (1996) Ploughing and splashing flows over submerged bodies of general shape. Paper presented at *Australian Mathematical Society Annual Conference*, Adelaide.

[8] Ting, L. & Keller, J. B. (1974) Planing of a flat plate at high Froude number. *Phys. Fluids* **17**, 1080–1086.

[9] Tuck, E. O. (1991) Ship-hydrodynamic free–surface problems without waves. *J. Ship Res.* **35**, 277–287.

[10] Vanden-Broeck, J.-M. & Dias, F. (1991) Nonlinear free–surface flows past a submerged inclined flat plate. *Phys. Fluids.* **A3**, 2995–3000.

[11] Wehausen, J. V. & Laitone, E. V. (1960) Surface waves. In: S. Flugge (ed.), *Handbuch der Physik* **9**. Springer-Verlag.